MODELING OF BULK HETERO JUNCTION SOLAR CELL

M.Sc Thesis
By
MAYSON ABDELMAGEED MANSOUR

A thesis submitted in partial fulfillment of the requirements for the degree of Master of Science in Physics

Under the supervision of
Prof. Mohammed Osman Sid Ahmed

Department of Physics
Faculty of Science
University of Khartoum
September 2007

بسم الله الرحمن الرحيم

قال تعالى :

و قل ربي زدني علما و ألحقنى بالصالحين

صدق الله العظيم

Dedication

To my parents, brothers and sisters.

To my dear husband.

To my lovely friend

Acknowledgment

Praise to Allah, the grateful cherishes, who bestowed health, strength and patience upon to conduct this work.

I wish to express my deep gratitude to my supervisor Prof. Mohammed Osman Sid Ahmed, for his continuous advice, patience and support.

I am also grateful to Ustaz Bushra .M.Omer, Ahlia University, Ustaz Sahar.S.aldeen, Khartoum University. And Ustaz Najwa Ibrahim, Electrical Engineering College for their help and support.

I am particularly thankful to the members of the Department of Physics ,Khartoum University, for their great help.

Contents

Page

Chapter One (Motivation and Outlines)

Chapter Two (Theory of the solar cell)

Chapter Three (Theories of computational methods)

Chapter Four (Material and Method)

Chapter Five (Results and calculations)

Chapter Six (The conclusion and recommendations)

List of Table

List of Figure

ملخص البحث:

درست كفاءة الخليه الشمسيه من خلال تعديل فرق جهد الدائره المفتوحه بإجراء إحدى طرق الحوسبه التجريبيه على شبه الموصل العضوي ((Polythiophene(PT) حيث شِوِب المركب بمجموعتي ألكيل(hexyl, and methyl) و عنصرين من الهلوجينات (البروم و اليود).

أوضحت النتائج أن كفاءة الخليه الشمسيه تناقصت بنسبة 10.3% عند إحلال مجموعة (hexyl) بدلا عن الهايدروجين في سلسلة شبه الموصل الهايدروكربوني (PT). وتناقصت بنسبة 15.4% عند إحلال الهايدروجين بمجموعة (methyl) مقارنة بالخليه المحتويه على شبه الموصل الأصيل.

ووجد أيضا أن كفاءة الخليه تزيد بنسبة 23.1% عند إحلال عنصر البروم بدلا عن الهايدروجين.وتزيد بنسبة 24.4% عند إحلال عنصر الهايدروجين بعنصراليود في سلسلة المركب العضوي (PT).

Abstract

The efficiency of bulk heterojunction solar cell is studied by optimizing the open circuit voltage, and by taking semi empirical calculations from polythiophene (PT). The (PT) is doped with some alkyls (methyl and hexyl) and two Halogens elements (Iodine and Bromine)

The results show that the efficiency of a solar cell of PT with hexyl group substituted for hydrogen atom is decreased by 10.3%. And with methyl group the decrease is about 15.4% from the cell of intrinsic polythiophene.

The efficiency of the solar cell is increased by 23.1% with Bromine substituted for hydrogen atom in PT, and is increased by 24.4% with Iodine substitution.

Chapter One

Motivation and Outlines

1.1 Motivation:

The limited supply of today's main energy sources(oil, coal, uranium) will force us sooner or later to replace most of the currently used power plants with renewable energy sources. According to recent predictions, [1], the inevitable permanent de-cline in the global oil production rate is expected to start within the next 10-20 years.

Worldwide, oil prices will then rise considerably favouring the introduction of various renewable energy sources such as the direct conversion of solar energy (solar cells), but also others like for example, hydroelectric and wind-power systems. However, the combustion of fossil fuels in the past has already harmful effects on the delicate balance of nature on our planet. Today, about 20.10^{12} Kg of carbon dioxide is put into the atmosphere every year, mainly by burning fossil fuel [2].

Today's plants are unable to absorb this huge amount of extra CO2. As a result the CO2 concentration in the atmosphere continues to mount, (Fig.1.1), adding considerably to the greenhouse effect which will increase the global mean surface temperature depending on future emission scenarios and the actual climate sensitivity by another 0.6-7.0ºC by the year 2100 [2].

Global mean surface temperature has increased by 0.3-0.6ºC since the late 19th century and the global sea level [2] has risen by 10-25cm, most likely due to human activities [1]. The consequences of this temperature change have already increased the frequency and severity of natural disasters [1] and are likely to have more devastating effects for humans and other life forms in all parts of Earth within the next decades.

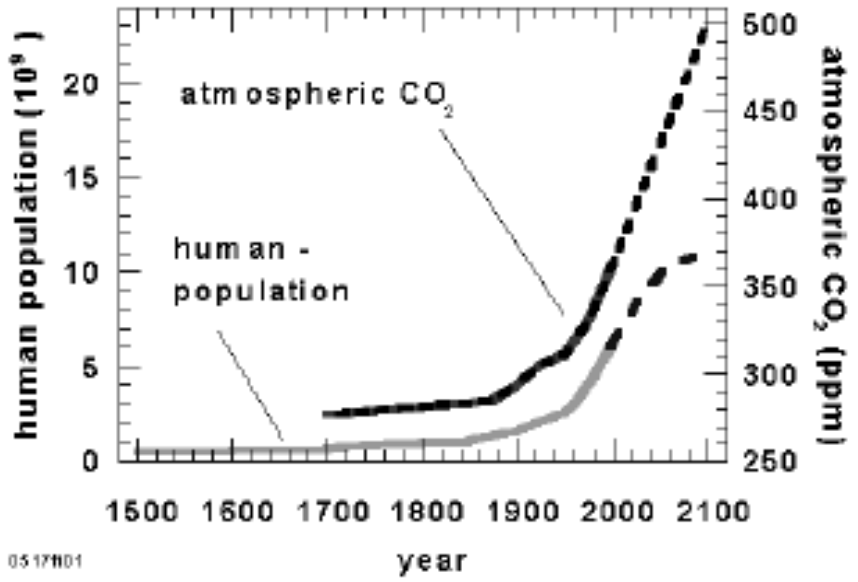

Figure 1.1: The atmospheric concentrations of green house gases like CO2 have grown significantly since pre-industrial times. This can be largely attributed to human activities, mostly fossil-fuel use. Dashed lines are possible (optimistic) future scenarios [1].

Among the renewable energy sources solar energy has a great importance. Sun has always been the most powerful energy sources on earth. It is clean, environmentally friendly and is free. The conversion of sunlight into electricity is performed by solar cells. The solar cell technology until recently was only based on inorganic semiconductor technology. 24% power conversion efficiencies [3] are achievable using inorganic semiconductor technology. However, cost effective techniques are required organic solar cells have been the low cost alternatives of inorganic solar cells. The organic, polymer based photovoltaic elements have introduced at least the potential of obtaining cheap and easy methods to produce energy from light [3]. The possibility of chemically manipulating the material properties of polymers (plastics) combined

with a variety of easy and cheap processing techniques has made polymers based materials present in almost every aspect of modern society [3]. The engineering of the electronic band gap of organic semiconductors by chemical synthesis and mobility's as high as 10 cm^2 /Vs [4] made them attractive and competitive with inorganic materials [5].

1.2 Inorganic solar cell:

The photovoltaic cells have been extensively studied since the 1950s [6]. When first crystalline silicon solar cell, which had an efficiency of 6%, was developed at Bell laboratories [6, 7]. Since then, the efficiency has reached 27% [8] for crystalline Si solar cell, which is already closed to the theoretical predicted upper limit of 30% [6].

Practically all conventional inorganic solar cells incorporate a semiconductor that is doped to form a p-n junction across which the photovoltaic is generated. The p-type contains an excess of positive charges (holes) and the n-type contains an excess of negative charge (electrons).

At present inorganic solar cell such as mono and multi – crystalline silicon have found markets for small scale devices such as solar panels on roofs, pocket calculators and water pumps. Today the production of inorganic solar cell requires many energy intensive processes at high temperature (400^o C -1400^o C) and high vacuum conditions with numerous lino graphic steps leading to relatively high manufacturing costs [8].

1.3 Organic solar cells:-

The first investigation of an organic PV cell came as early as 1959, when a single crystal cell was studied [3]. The cell exhibited a photo voltage of 200mV with an extremely low efficiency [4]. Since then, many

years of research have shown that the typical power conversion efficiency of PV devices based on single organic materials will remain below 0.1%. Primarily, this is due to the fact that absorption of light in organic materials almost always results in the production of a mobile excited state (referred to an exciton), rather than free electron-hole pairs as produced in inorganic solar cells. This occurs for the reason that organic materials are characterized by low dielectric constant (typically 2-4), compared to inorganic semiconductors, which require an energy input much higher than the thermal energy (kT) to dissociate these excitons [3]. The electric field provided by the asymmetrical work functions of the electrodes is not sufficient to break-up these photo generated excitons. Instead, the excitons diffuse within the organic layer until they reach the electrode, where they may dissociate to supply separate charges, or recombine. Since the exciton diffusion lengths are typically 1-10 nm [3], being much shorter than the device thicknesses, exciton diffusion limits charge carrier generation in these devices since most of them are lost through recombination. Photo generation is therefore a function of the available mechanisms for excitons dissociation. A major breakthrough in the cell performance came in 1986 when Tang discovered that much higher efficiencies (about 1%) are attainable when bringing an electron donor and an electron acceptor together in one cell [3]. This concept of heterojunction is the heart of all three currently existing types of organic PV cells: dye-sensitized solar cells, planar organic semiconductor cells, and high surface area, or bulk heterojunction cells [3].

1.4 Outline of the thesis:

Chapter two is aimed to give a more comprehensive insight into the important theories of a solar cell and details about organic solar cell and its operation principle. Chapter three shows all computational methods used in the research of the properties of the matter, and discuss the theory behind Mopac. Chapter four is the material and method, in this chapter we discusses the dependence of the open circuit voltage on the energy levels, and give a literature review about polythiophene material. In chapter five the results and calculations was presented, finally the conclusion and recommendations are given in chapter six.

Chapter Two
Theory of the solar cell

2.1 The p-n junctions:

A p-n junction consists of two semiconductor regions with opposite doping type as shown in Figure (2.1) .The dopants are assumed to be shallow, so that the electron (hole) density in the n-type (p-type) region is approximately equal to the donor (acceptor) density, at room temperature.

p-n junctions are of great importance both in modern electronic applications and in understanding other semiconductor devices. The p-n junction theory serves as the foundation of the physics of semiconductor devices. The basic theory of current-voltage characteristics of p-n junctions was established by Shockley, [9]. This theory was then extended by Sah, Noyce, and Shockley [10], and by Moll, [11]. The basic equations presented in section 2.2 are used to develop the ideal static and dynamic characteristics of p-n junctions.

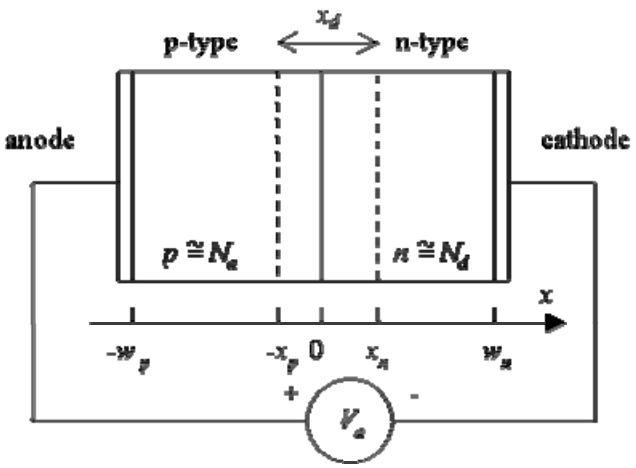

Figure (2.1) semiconductor regions with opposite doping type

2.2 Basic Equations

The basic equations for semiconductor-device operation describe the static and dynamic behavior of carriers in semiconductors under external influences, such as applied field or optical excitation, that cause deviation from the thermal-equilibrium condition,[22] The basic equations can be classified in three groups; electrostatic equations, current-density equations, and continuity equations.

2.2.1 Electrostatic Equations:

There are two important equations relating charge to electric field. The first is from one of Maxwell equations,

$$\nabla . D = p(x, y, z) \qquad \textbf{(2.1)}$$

where D is electric displacement

also known as Gauss' law or Poisson equation. For a one-dimensional problem, this reduces to a more useful form of

$$\frac{d^2 \psi_i}{dx^2} = -\frac{d\mathscr{E}}{dx} = -\frac{\rho}{\varepsilon_s} = \frac{q(n - p + N_A - N_D)}{\varepsilon_s} \qquad \textbf{(2.2)}$$

($\psi_i = -E_i / q$).This is commonly used, for example, to determine the potential and field distribution caused by a charge density p within the depletion layer. The second equation deals with charge density along an interface, instead of bulk charge.

2.2.2 Current-Density Equations:

The most-common current conduction consists of the drift component, caused by the electric field, and the diffusion component, caused by the carrier-concentration gradient. The current-density equations are:

$$\boldsymbol{J}_n = q\mu_n n\boldsymbol{\mathscr{E}} + qD_n \nabla n \qquad \textbf{(2.3)}$$

$$\boldsymbol{J}_p = q\mu_p p\boldsymbol{\mathscr{E}} - qD_p \nabla p \qquad \textbf{(2.4)}$$

$$\boldsymbol{J}_{\text{cond}} = \boldsymbol{J}_n + \boldsymbol{J}_p \qquad \textbf{(2.5)}$$

Where, J_n and J_p are the electron and hole current densities, respectively. The (μ_n and μ_p) is the electron and hole mobilities . For non-degenerate semiconductors the carrier diffusion constants (D_n and D_p) and the mobilities are given by the Einstein relation [$D_n = (KT/q)\mu_n$ etc.]. For a one-dimensional case, Eqs. 2.3 and 2.4 reduce to

$$J_n = q\mu_n n\mathscr{E} + qD_n\frac{dn}{dx} = q\mu_n\left(n\mathscr{E} + \frac{kT}{q}\frac{dn}{dx}\right) = \mu_n n\frac{dE_{Fn}}{dx} \qquad \textbf{(2.6)}$$

$$J_p = q\mu_p p\mathscr{E} - qD_p\frac{dp}{dx} = q\mu_p\left(p\mathscr{E} - \frac{kT}{q}\frac{dp}{dx}\right) = \mu_p p\frac{dE_{Fp}}{dx} \qquad \textbf{(2.7)}$$

where E_{Fn} and E_{Fp} are quasi Fermi levels for electrons and holes, respectively. These equations are valid for low electric fields. At sufficiently high fields the term $\mu_n\xi$ or $\mu_p\xi$ should be replaced by the saturation velocity v_s , (and the last equalities about E_{Fn} and E_{Fp} do not hold any more). These equations do not include the effect from an externally applied magnetic field where the magneto-resistive effect reduces the current.

2.2.3 Continuity equations:

While the above current-density equations are for steady state conditions, the continuity equations deal with time-dependent phenomena such as low-level injection, generation and recombination. Qualitatively, the net change of carrier concentration is the difference between generation and recombination, plus the net current flowing in and out of the region of interest. The continuity equations

$$\frac{\partial n}{\partial t} = G_n - U_n + \frac{1}{q}\nabla \cdot \boldsymbol{J}_n \qquad \textbf{(2.8)}$$

$$\frac{\partial p}{\partial t} = G_p - U_p - \frac{1}{q}\nabla \cdot \boldsymbol{J}_p \qquad \textbf{(2.9)}$$

where G_n and G_p are the electron and hole generation rate respectively, caused by external influences such as the optical excitation with photons or impact ionization under large electric fields. And the recombination rates, $U_n = \Delta n / \tau_n$, and $U_p = \Delta p / \tau_p$.

for the one-dimensional case under a low-injection condition, Eqs. 2.8 and 2.7 reduce to

$$\frac{\partial n_p}{\partial t} = G_n - \frac{n_p - n_{po}}{\tau_n} + n_p \mu_n \frac{\partial \mathscr{E}}{\partial x} + \mu_n \mathscr{E} \frac{\partial n_p}{\partial x} + D_n \frac{\partial^2 n_p}{\partial x^2} \qquad \textbf{(2.10)}$$

$$\frac{\partial p_n}{\partial t} = G_p - \frac{p_n - p_{no}}{\tau_p} - p_n \mu_p \frac{\partial \mathscr{E}}{\partial x} - \mu_p \mathscr{E} \frac{\partial p_n}{\partial x} + D_p \frac{\partial^2 p_n}{\partial x^2} \qquad \textbf{(2.11)}$$

2.3 Current- voltage characteristics:

The ideal current-voltage characteristics are based on the following four assumptions: (1)The abrupt depletion-layer approximation; that is, the built-in potential and applied Voltages are supported by a dipole layer with abrupt boundaries, and outside the boundaries the semiconductor is assumed to be neutral; (2)The Boltzmann approximation, (3) the low-injection assumption; that is, the injected minority carrier densities are small compared with the majority-carrier densities; and (4) no generation-recombination current exists inside the depletion layer, and the electron and hole currents are constant throughout the depletion layer. We first consider the Boltzmann relation at thermal equilibrium

$$n = n_i \exp\left(\frac{E_F - E_i}{kT}\right) \qquad (2.12)$$

$$p = n_i \exp\left(\frac{E_i - E_F}{kT}\right) \qquad (2.13)$$

Where n and p is the electron and hole carrier density E_F, E_i is Fermi energy and intrinsic energy level.

Obviously, at thermal equilibrium, the pn product from the above equations is equal to n_i^2. When voltage is applied, the minority-carrier densities on both sides of the junction are changed, and the pn product is no longer equal to n_i^2 we shall now define the quasi-Fermi levels as follows:

$$n \equiv n_i \exp\left(\frac{E_{Fn} - E_i}{kT}\right) \qquad (2.14)$$

$$p \equiv n_i \exp\left(\frac{E_i - E_{Fp}}{kT}\right) \qquad (2.15)$$

Where E_{Fn} and E_{Fp} are the quasi-Fermi levels for electrons and holes, respectively. From Eqs.2.14and 2.15 we obtain

$$E_{Fn} \equiv E_i + kT\ln\left(\frac{n}{n_i}\right) \qquad (2.16)$$

$$E_{Fp} \equiv E_i - kT\ln\left(\frac{p}{n_i}\right) \qquad (2.17)$$

The product pn becomes

$$pn = n_i^2 \exp\left(\frac{E_{Fn} - E_{Fp}}{kT}\right) \qquad (2.18)$$

For a forward bias, $(EFn - EFp)\rangle 0$ and $pn\rangle n_i^2$; on the other hand for a reversed bias $(EFn - EFp)\langle 0$ and $pn\langle n_i^2$

From Eq.2.6 and Eq. 2.14, and the fact that $\xi = \nabla E / q$ we obtain

$$\begin{aligned} \boldsymbol{J}_n &= q\mu_n\left(n\mathscr{E} + \frac{kT}{q}\nabla n\right) = \mu_n n\nabla E_i + \mu_n kT\left[\frac{n}{kT}(\nabla E_{Fn} - \nabla E_i)\right] \\ &= \mu_n n\nabla E_{Fn} \ . \end{aligned} \qquad (2.19)$$

Similarly, we obtain,

$$\boldsymbol{J}_p = \mu_p p\nabla E_{Fp} \qquad (2.20)$$

Thus, the electron and hole current densities are proportional to the gradients of the electron and hole quasi-Fermi levels, respectively. If $E_{Fn} = E_{Fp} = cns\tan t$ (at thermal equilibrium), then $J_n = J_p = 0$.

The variations of E_{Fn} and E_{Fp} with distance are related to the carrier concentrations as given in Eqs. 2.16and 2.17, and to the current as given by Eqs. 2.19 and 2.20. Inside the depletion region, E_{Fn} and E_{Fp} remain relatively constant. This comes about because the carrier concentrations

are relatively much higher inside the depletion region, but since the currents remain fairly constant, the gradients of the quasi-Fermi levels have to be small. In addition, the depletion width is typically much shorter than the diffusion length, so the total drop of quasi-Fermi levels inside the depletion width is not significant.

With these arguments, it follows that within the depletion region,

$$qV = E_{Fn} - E_{Fp} \tag{2.21}$$

Equations 2.18 and 2.21 can be combined to give the electron density at the boundary of the depletion-layer region on the p-side ($x = -W_{Dp}$):

$$n_p(-W_{Dp}) = \frac{n_i^2}{p_p}\exp\left(\frac{qV}{kT}\right) \approx n_{po}\exp\left(\frac{qV}{kT}\right) \tag{2.22}$$

Where $p_p \approx p_{po}$ for low level injunction and n_{po} is the equilibrium electron density on the p-side. Similarly,

$$p_n(W_{Dn}) = p_{no}\exp\left(\frac{qV}{kT}\right) \tag{2.23}$$

Where $x = W_{Dn}$ for the n-type boundary. The preceding equations are the most-important boundary conditions for the ideal current-voltage equation. From the continuity equations we obtain for the steady-state condition in the n-side of the junction:

$$-U - \mu_p \mathscr{E}\frac{dp_n}{dx} - \mu_p p_n \frac{d\mathscr{E}}{dx} + D_p \frac{d^2 p_n}{dx^2} = 0 \tag{2.24}$$

$$-U + \mu_n \mathscr{E}\frac{dn_n}{dx} + \mu_n n_n \frac{d\mathscr{E}}{dx} + D_n \frac{d^2 n_n}{dx^2} = 0 \tag{2.25}$$

In these equations, U is the net recombination rate. Note that due to charge neutrality, majority carriers need to adjust their concentrations such that $(n_n - n_{n0}) = (p_n - p_{no})$ it also follows that $dn_n / dx = dp_n / dx$

Multiplying Eq. 2.23 by, $\mu_p p_n$ and Eq. 2.24 by, $\mu_n n_n$, and combining with the Einstein relation D = (kT/q)μ, we obtain

$$-\frac{p_n - p_{no}}{\tau_p} - \frac{n_n - p_n}{(n_n/\mu_p) + (p_n/\mu_n)} \mathscr{E} \frac{dp_n}{dx} + D_a \frac{d^2 p_n}{dx^2} = 0 \qquad (2.26)$$

Where

$$D_a = \frac{n_n + p_n}{n_n/D_p + p_n/D_n} \qquad (2.27)$$

is the am bipolar diffusion coefficient, and

$$\tau_p \equiv \frac{p_n - p_{no}}{U} \qquad (2.28)$$

From the low-injection assumption Eq. 2.26 reduces to

$$-\frac{p_n - p_{no}}{\tau_p} - \mu_p \mathscr{E} \frac{dp_n}{dx} + D_p \frac{d^2 p_n}{dx^2} = 0 \qquad (2.29)$$

Which is Eq. 2.25 except that the term $\mu_p p_n d\xi / dx$ is ignored under the low-injection assumption

In the neutral region where there is no electric field, Eq. 2.28 further reduces to

$$\frac{d^2 p_n}{dx^2} - \frac{p_n - p_{no}}{D_p \tau_p} = 0 \qquad (2.30)$$

The solution of Eq. 2.29, with the boundary conditions of Eq. 2.22,and $p_n(x = \infty) = p_{no}$ gives

$$p_n(x) - p_{no} = p_{no}\left[\exp\left(\frac{qV}{kT}\right) - 1\right]\exp\left(-\frac{x - W_{Dn}}{L_p}\right) \qquad (2.31)$$

Where

$$L_p \equiv \sqrt{D_p \tau_p} \tag{2.32}$$

At $x = W_{Dn}$ the hole diffusion current is

$$J_p = -qD_p \left.\frac{dp_n}{dx}\right|_{W_{Dn}} = \frac{qD_p p_{no}}{L_p}\left[\exp\left(\frac{qV}{kT}\right) - 1\right] \tag{2.33}$$

Similarly, we obtain the electron diffusion current in the p-side

$$J_n = qD_n \left.\frac{dn_p}{dx}\right|_{-W_{Dp}} = \frac{qD_n n_{po}}{L_n}\left[\exp\left(\frac{qV}{kT}\right) - 1\right] \tag{2.34}$$

. It is interesting to note that the hole current is due to injection of holes from the p-side to the n-side, but the magnitude is determined by the properties in the n-side only D_p, L_p, p_{po} .The analogy holds for the electron current. The total current is given by the sum of Eqs. 2.33, and 2.34:

$$J = J_p + J_n = J_0\left[\exp\left(\frac{qV}{kT}\right) - 1\right] \tag{2.35}$$

The current voltage characteristics of a solar cell in the dark and under illumination are shown in Fig 2.2.

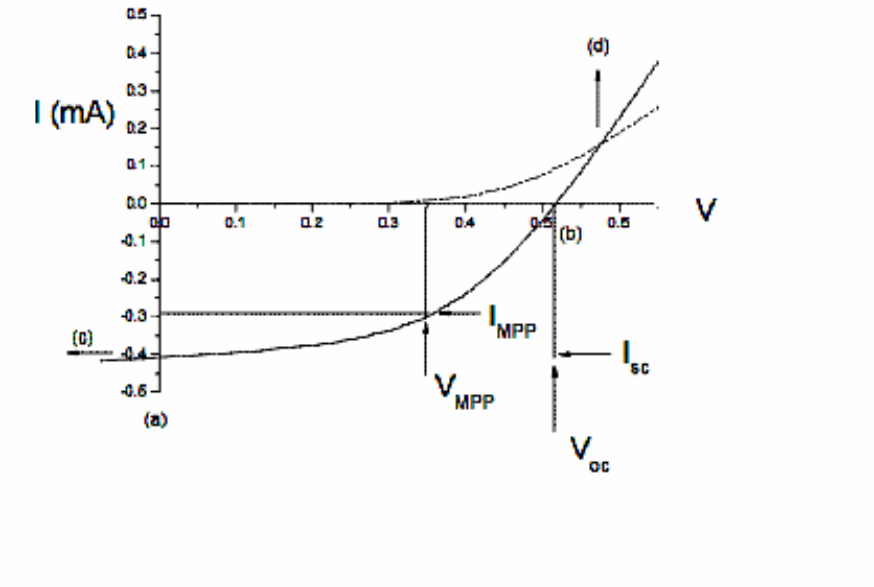

Fig 2.2current-voltage (I-V) curves of an organic solar cell (dark, dashed; illumination, full line).the characteristic intersection with the abscissa and ordinate are the open circuit voltage (Voc) and the short circuit current (I^{SC}) respectively.

In the dark, these is almost no current Flowing, until the contacts start to inject heavily at forward bias for voltages larger than the open circuit voltage (a) short circuit current condition where the maximum generated photocurrent flows (b) flat band condition where the photo generated current is balanced to zero. The fourth quadrant (between (a) and (b) the device generates power). At maximum power point (MPP), the product of current and voltage is the largest [12].

The largest power out put (P_{max}) is determined by the point where the product of voltage and current is maximized. Division of P_{max} by the product of I_{sc} and v_{oc} yields the Fill Factor FF. what determines the FF is question of how many generated charge carriers can actually reach the electrodes, when the built in field is lowered to wards the open circuit voltage [12].

The photovoltaic power conversion efficiency of a solar cell is determined by the following formula:

$$\eta_e = V_{oc} \frac{* I_{sc} * FF}{P_{in}} (2.36)$$

$$FF = \frac{I_{mpp} * V_{mpp}}{I_{sc} * V_{oc}} (2.37)$$

where $\mathbf{V_{oc}}$ is the open circuit voltages I_{sc} is the short circuit current, FF is the Fill factor an P_{in} is the incident light power density, which is standardized at $1000 W/m^2$ For solar cell testing with a spectral intensity distribution matching that of the sun on the earth's surface at an incident angle of 48.2^0, which is called the AM 1.5 spectrum [13]. I_{mpp} and V_{mpp} are the current and voltage at the maximum power point in the Fourth quadrant of the current-voltage characteristics.

2.4 organic solar cells:

Atypical organic solar cell consists of photo active layer sandwiched between two different electrodes, one of which should be transparent in order to allow the incoming photons to reach the photoactive layer [2] as seen in Fig 2.3

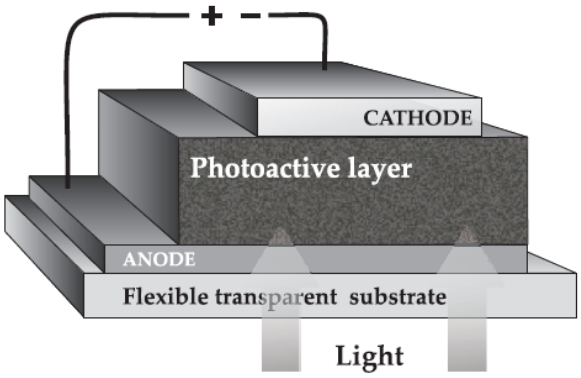

Figure 2.3: Schematic layout of an organic solar cell.

The photoactive layer mainly consist of two organic materials one of which is a donor (gives electron) and the other is an accepters (accepts electrons). Conjugated polymers as donor and fullerene as acceptors are generally employed in organic solar cell [12].

Organic electronic materials are conjugated molecular solids where both optical absorption and charge transport are dominated by partly delocalized π and π^* orbital. The flexibility of chemical tailoring of desired properties such as band gaps as well as the easy and cheap processing and accessibility of conjugated polymers made them competitive and attractive [12].

2.5 Material of organic solar cell:

One class of organic materials used as photoactive layer in bulk heterojunction PV cells that have received considerable attention in the last few years are conjugated polymer. They combine the opto-electronic properties of conventional semiconductors with the excellent mechanical and processing properties of 'plastic' materials. Additionally, they possess an unprecedented flexibility in the synthesis, allowing for alteration of a wide range of properties, such as band gap, molecular orbital energy level, wetting and structural properties, as well as doping. This ability to design and synthesize polymers and molecules that can be casted from solution using wet-processing techniques such as spin-coating, ink jet printing, and screen printing, represents an enormous attractive route for cheap production of large-area PV cells that can be applied to systems that require flexible substrates. Since ultra fast photo induced electron transfer from a conjugated polymer as donor to C60 or its derivatives as acceptor was first observed in 1992 by Sariciftci et al. [3].

Conjugated polymers are organic compound (often called organic conductors) contain extended π-conjugated system single and double bonds alternating a long the polymer chain. Conjugated polymer exhibit a high potential for production of efficient and, at the same time, low cost, flexible optoelectronic devices with option for large area application [14].

It is generally agreed that the mechanism of conductivity in conducting polymers is based on the motion of charged defects within the conjugated frame work. The charge carrier either positive or negative, are the products of oxidation or reduction of the polymers. It is the charge carrier mobility that leads to the high conductivity of these polymers. The conductivity σ of a conducting polymer is generally related to the number of charge carriers n and their mobility μ.

$$\sigma \propto n\mu \qquad (2.38)$$

Because the band gap of conjugated polymers is large $(\geq 1.9ev)$, as a consequence it only absorbs at wave lengths >650nm [12]. The essential structure of all conjugated polymer is qusi-infinite π - system extending over a large number of resuming monomer units. The structure of polythiophene is shown in Fig (2.3)

(a) (b)

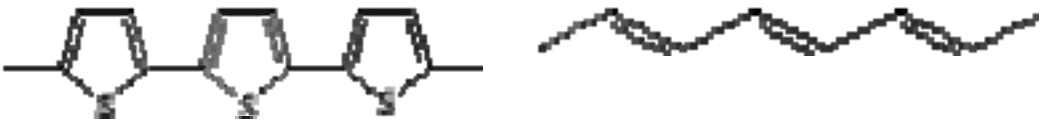

Fig. 2.4 (a) polythiophenes (PTs) structure (b) polyacytelene (PA) structure

The molecular orbital theory defines that when two atoms bond to form a molecule, the atomic orbital overlap to form a molecular orbital (bonding and anti bonding). The electrons occupy these molecular orbital according to the Pawli Exclusion principle the difference between the

highest occupied molecular orbital (HOMO) and the lowest unoccupied molecular orbital (LUMO) is assigned as the energy band gap of the material. The HOMO and LUMO level is on analogous to valance band and conduction band in inorganic materials.

2.6 Bulk heterojunction solar cell (BHJ):

Most of the developments that have improved the performance of organic PV devices are based on donor-acceptor heterojunction (HJ). The idea behind a (HJ) is to use two materials with different electron affinities and ionization potentials. At the interface, the resulted potentials are strong and may favor exciton dissociation: the electron will be accepted by the material with the larger electron affinity and the hole by the material with the lower ionization potential, provided that the differences in potential energy are larger than the exciton binding energy. In the planar (HJ), or 'bi-layer' device, the organic donor-acceptor interface separates excitons much more efficient than an organic/metal interface in the single layer device.

The energetic diagram of such a bi-layer device is depicted in Fig.2.5(a). Sunlight photons which are absorbed inside the device excite the donor molecule, leading to the creation of excitons. The created excitons start to diffuse within the donor phase and if they encounter the interface with the acceptor then a fast dissociation takes place leading to charge separation [3]. The resulting metastable electron-hole pairs across the donor acceptor interface may still be Coulombically bound and an electric field is needed to separate them into free charges [3]. Therefore, at typical operation conditions, the photon-to-free-electron conversion efficiency is not maximal. Subsequently, the separated free electrons (holes) are transported with the aid of the internal electric field, caused by the use of electrodes with different work functions, towards the cathode (anode) where they are collected by the electrodes and driven into the

external circuit. However, the excitons can decay, yielding e.g. luminescence, if they are generated far from the interface. Thus, the excitons should be formed within the diffusion length of the interface. Since the exciton diffusion lengths in organic materials are much shorter than the absorption depth of the film, this limits the width of effective light-harvesting layer.

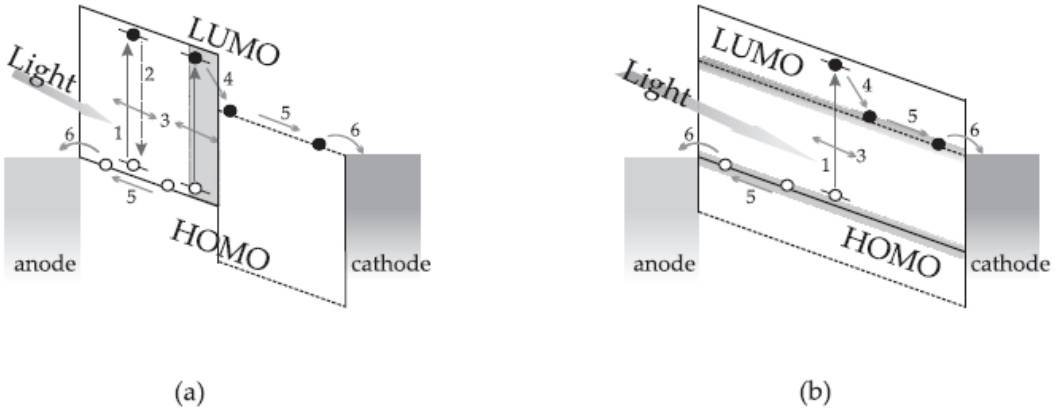

Fig. 2.5: Schematic band diagram of a bi-layer device (a) and a bulk heterojunction (b). The dashed line represents the energy levels of the acceptor, while the full lines indicate the energy level of the donor in the PV cell.

A revolutionary development in organic PVs came in the mid 1990s with the introduction of the dispersive (or bulk) heterojunction, where the donor and acceptor material are blended together. If the length scale of the blend is similar to the exciton diffusion length, the exciton decay processes is dramatically reduced since in the proximity of every generated exciton there is an interface with an acceptor where fast dissociation takes place. Hence, charge generation takes place everywhere in the active layer, as is schematically represented in Figure

2.5(b). Provided that continuous pathways exist in each material from the interface to the respective electrodes, the photon-to-electron conversion efficiency and, hence, the photosensitivity is dramatically increased. The observation of improved device performance using bulk heterojunctions represents the departure from the device physics of conventional inorganic PV cells and has led to new device and materials designs. Nowadays, the bulk heterojunction is the most promising concept for all-organic PV cells. Dye-sensitized solar cells, as developed in 1990s by Gratzel, however, function on similar principles [3].

2.7 Operation Principles:-

The principles of operation of organic solar cells mainly consist of the following steps: (i) absorption of light (ii) charge separation (iii) charge transport to the electrodes. Absorption of light by an organic material leads to bound electron and hole pairs which can be regarded as excitons. These excitons have to be separated into free charge carriers. A driving force is necessary for the charges to reach the electrodes. In a donor-acceptor junction, generally a gradient in chemical potentials of electrons and holes is built up that is the difference between the HOMO level of the donor and the LUMO level of the acceptor [12]. The maximum open circuit voltage (Voc) is determined by this internal electric field which contributes to a field induced drift of charge carriers. The electrodes need to have two different work functions, one low work function metal for the collection of electrons and one high work function metal for the collection of the holes. Another driving force can be the concentration gradients of the respective charges which lead to a diffusion current. The transport of charges is affected by recombination during the journey to the electrodes, particularly if the same material serves as transparent medium for both electrons and holes [12].

As a last step, charge carriers are extracted from the device through two selective contacts. A transparent Indium tin oxide (ITO) coated substrate with work functions around 5ev versus vacuum , matching the HOMO levels of most of the conjugated polymers (hole contact), is used on the illumination side, and an evaporated thin lithium fluoride / aluminum metal. Contact with a work function of around 4.3eV matching the LUMO of acceptor PCBM (electron contact), is used in general on the other side.

.

Chapter Three

Theories of computational methods

3.1 Introduction:

Computational chemistry and material science spans a wide range of activities from quantum mechanical calculation to classical mechanical – simulation, to chemical engineering problems with fluid dynamic implication [15]. In short terms computational chemistry problems involve the formulation and solution of molecular models as the result of mathematical equations able to describe the system of interest.

Not so far in the past, chemical modeling was accomplished with plastic models, now a day it is performed via computer. In this way it is possible to access molecular information useful for predicting properties and uses of given chemical system.

It is important to underline the power of modeling in research, as predictions of properties and reactions behavior to be available before the compounds are made, saving research and development costs. More over molecular modeling can be used for research and educational purposes, allowing students to build dynamic models of compounds and providing a method to visualize molecular geometries and to demonstrate chemical principles. Mathematical models used to describe a chemical system can be of different kinds, the basic ones that we can mention here are:

3.1.1 Ab inito:

This method tries to solve Schrödinger's equation using only standard mathematical approximations, with no inclusion of experimental data, [15].

3.1.2 Semi empirical:

This method uses experimental data to simplify the Schrödinger's equation, to solve it more quickly, [15].

3.1.3 Molecular Mechanics:

This method is described by the Ab inito and Semi empirical methods. In this case simple algebraic expressions are used to calculate the total energy of compound, without solving the wave function [15]. Constants in these equations are obtained from experimental data or from Ab inito calculations.

The following programs are used to calculate the properties of the molecular modeling with the above mentioned methods:-

Gaussian 03, Gamess, PCGAMESS, GAMESS UK, Molpro, Nwchem, achen ACEsII, COLOUMBUS, Mocals, Dalton, Argus Lab, Mopac6, WinMopac, AMpac, MSINDO,[64].

In this work the semi empirical method has been selected, because both Ab inito and Molecular mechanics needs computer network with special features which is difficult to be provided. Also it takes long time to make the calculations and give the result. Although Semi empirical is not accurate enough, yet it can give a good prediction of the properties of molecular system. Here Mopac program used to operate this method.

3.2 semi empirical theory:

There are five distinct methods available within Mopac: MINDO\3, MNDO, AMI, PM3 and MNDO-d. All are semi empirical, and have roughly the same structure. A complete knowledge of these methods is not necessary in order to use Mopac; however a superficial understanding of these methods and their relationship to Ab inito methods are important for using Mopac and particularly for interpreting the results, [15].

The Five methods have many features in common. They are all Self- Consistent Field (***SCF***) methods. They take into account electrostatic repulsion and exchange stabilization, and in them, all calculated integrals are evaluated by approximate means. Further, they all use a restricted basis set of one ***s*** orbital and three ***p*** orbital ($\boldsymbol{P_x}$,$\boldsymbol{P_y}$ and $\boldsymbol{P_z}$) per atom (except MNDO-d which has five ***d*** orbital in addition to the ***s-p*** basis set) and ignore overlap integrals in the secular equation[65]. Thus instead of solving

$$|H - ES| = 0$$

The expression

$$|H - E| = 0$$

In Which ***H*** is the secular determinant, ***S*** is the overlap matrix, and ***E*** is the set of eigen values, is solved. These approximations considerably simplify quantum mechanical calculations on systems of chemical interest. As a result, larger systems can be studied. Computational methods are only models, and there is no advantage in rigorously solving Schrödinger's equations or a large system if that system had to be abbreviated in order to make the calculation treatable. Semi empirical methods are thus seen to be well balanced; they are accurate enough to have useful predictive powers, yet fast enough to allow large systems to be studied.

All five semi empirical methods contain sets of parameters. For MINDO\3 atomic parameters exist, while MNDO, AM1, PM3, and MNDO-d use only single atom parameters. Not all parameters are optimized for all methods. Also all Five semi empirical methods use two experimentally determined constants per atom, the atomic mass of the most abundant isotope and the heat of atomization.

3.3 Terminology and description of Mopac:

Mopac is a general purpose semi empirical molecular orbital package for the study of solid state and molecular structure and reactions. Semi empirical Hamiltonians MNDO, MINDO/3, AM1, PM3, and MNDO-d are used in the electronic part of the calculation to obtain molecular orbital, the heat of formation and its derivative with respect to molecular geometry. Using these results Mopac calculates the vibration spectra, thermodynamics quantities, isotopic substitution effects and force constants for molecules, radicals, ions and polymers, [15].

While Mopac calls upon many concepts in quantum theory and thermodynamics, and uses some fairly advanced mathematics, the user needs to be familiar with these specialized topics. The input data are kept as simple as possible, so users can give their attention to the chemistry involved and not concern themselves with quantum and thermodynamics exotica.

The simplest description of how Mopac works is that the users creates a data file which describes a molecular system and specifies what kind of calculations and output desired. The user then commands Mopac to carry out the calculation using the data file. Finally the user extracts the desired output on the system from output files created by Mopac.

The name Mopac should be understood to mean" **M**olecular **O**rbital **P**ackage". The origin of the name is some what unusual, and might be of general interest.

3.4 Use of Mopac as an educational tool:

Although Mopac is designed as a research tool, a secondary, and still important, objective is that it should be suitable for educational purpose. The following list illustrates the types of topic which Mopac can be used for:

3.4.1 Semi empirical Theory:

Hamiltonians Matrices, one and two electron integrals, semi empirical methods , secular determinants, Diagonalization Eigen Vector, Eigen values, orthonormalization, density matrices, electronic energy, and the heat of formation (ΔH_f).

3.4.2 Symmetry theory:

Point-Groups, Irreducible representation, Normal Modes, Electronic states, symmetry products, space groups, little groups, and complex characters.

3.4.3 Electronic states:

Space and the spin quantization, Brillouin's Theorem, configurations interaction, shift operators, spin operators, Franck–Condon principles, Fluorescence, Red–shift, Pauli principle.

3.4.4 Normal Coordinates:

Infrared active models–reduced masses.

3.4.5 Time dependent Phenomena.

3.5 Geometry optimization:-

One of most common operations in computational chemistry is optimizing the geometry. This involves modifying the geometry until the energy is the minimum. At that point, the net forces acting on every atom vanish. Over the years, various methods for optimizing geometries have been developed. One of these, Baker's Eigen following procedure, has

proven to be very robust, and this is now used as the default. If for any reason, the EF method is not wanted, other methods are available.

The type of species that Mopac can optimize is the atoms, molecules, ions, and polymers.

Regular polymer systems for which periodic boundary Condition can be imposed can be calculated. The time for such calculations is about 30% greater than for a discrete molecule of the same size as the unit cell used geometries, including unit cell length can be optimized.

3.6 Electronic structure (Brillouin zone):

A Utility Program for analyzing the electronic structure of polymers, layer systems, and solid is provided. This uses output from Mopac, the space group symmetry operations, and interactive user input to generate the little groups for points in *k*–space, band structures, and cross section through *k*-space for selected bands. The first step in this analysis is to obtain the symmetry of the energy matrix for the solid. After this is done, the resulting structures in *k*-space are fully symmetry adapted.

3.7 Approximations used in MNDO, MNIDOI3, AM1, PM3and MNDO-d:

MINDO\3 stands for modified intermediate neglect of differential overlap, version3. MNDO stands for modified neglect of diatomic overlap, and AM1 is Austin model1. These are the first two of the MNDO type methods. PM3 is the modified neglect of diatomic overlap. Parametric methods number3, and MNDO-d, is really just MNDO with ***d*** orbital.

All these methods belong to the family of NDDO (Neglect of diatomic differential overlap) methods. In these methods all terms arising

from the overlap of two atomic orbital which are on different centers or atoms are set to zero. As this is not the form for developing the ideals of hartree-fock theory, the derivation of the Roothan-Hall equations will be assumed and our description of the method will start with the final Roothan-Hall equations (15).

3.7.1 Basic Roothaan – Hall equations:

Secular equations:

$$Ci|F - E_i S|Ci = 0 \qquad (3.3)$$

where:

$\boldsymbol{C}\equiv$Eigen vector, $\boldsymbol{S}\equiv$over lap matrix, $\boldsymbol{F}\equiv$ fock matrix, $\boldsymbol{E}\equiv$Eigen values

The total electronic energy of the system is given by:

$$E = \tfrac{1}{2} P(H + F) \qquad (3.4)$$

In which

$\boldsymbol{P}\equiv$density matrix

$\boldsymbol{H}\equiv$one electron matrix.

The general Fock matrix element is:

$$F_{\mu\upsilon}^{\alpha} = H_{\mu\upsilon} + \sum_{\lambda}\sum_{\sigma}(P_{\lambda\sigma}^{\alpha+\beta} < \mu\upsilon/\lambda\sigma > -P_{\lambda\sigma}^{\alpha} < \mu\lambda/\upsilon\sigma >) \qquad (3.5)$$

Or, spin-free

$$F_{\mu\upsilon}^{\alpha} = H_{\mu\upsilon} + \sum_{\lambda}\sum_{\sigma}(P_{\lambda\sigma} < \mu\upsilon/\lambda\sigma > -\tfrac{1}{2} P_{\lambda\sigma} < \mu\lambda/\upsilon\sigma >) \qquad (3.6)$$

All the methods use a minimum basis set consisting of maximum of one atomic orbital for each angular quantum number. The normal basis set for any atom consists of ones and three ***P*** orbital (P_x , P_y, and P_z).

3.7.2 Neglect of diatomic over lab integrals:

All overlap integrals arising from the overlap of two different atomic orbital are neglected. This reduces the overlap matrix to a unit matrix. The secular equation thus reduces to:

$$C_i = |F - E_i|C_i = 0 \qquad (3.7)$$

In semi empirical theory the Coulson density matrix is used e.g.:

$$P^{\alpha}_{\lambda\sigma} = \sum_{i}^{occ} C^{\alpha}_{\lambda i} C^{\alpha}_{\sigma i} \qquad (3.8)$$

where the sum is over all occupied spin molecular orbital Restricted Hartree - Fock (RHF) calculations, only the total density matrix is calculated:

$$P_{\lambda\sigma} = 2\sum_{i}^{occ} C_{\lambda i} C_{\sigma i} \qquad (3.9)$$

where the sum overall occupied molecular orbital.

When a system has more than half the available M.O.S.N, filled, it is computationally faster to calculate the positron electron equivalent:

$$P^{\alpha}_{\mu\upsilon} = 1 - \sum_{i=occ+1}^{N} C^{\alpha}_{\lambda i} C^{\alpha}_{\sigma i} \qquad (3.10)$$

$$P_{\mu\upsilon} = 2 - 2\sum_{i=occ+1}^{N} C_{\lambda i} C_{\sigma i} \qquad (3.11)$$

An important exception to this rule is the calculation of the one-electron two-center integrals $H_{\mu\upsilon}$, which is approximated by:

$$H_{\mu\upsilon} = S_{\mu\upsilon} 1/2\left(U_{\mu\mu} + U_{\upsilon\upsilon}\right) \qquad (3.12)$$

Where $S_{\mu\upsilon}$ is the overlap integrals between atomic orbital Ψ_{μ} on an atom, and Ψ_{υ} on another atom, and the U values are atomic orbital constant, supplied as data.

3.7.3 Self consistent field calculation:

Once all the integrals needed are calculated, the *SCF* calculation can be started. A trial density is constructed; this is a diagonal matrix with

the diagonal terms chosen so that every atom starts off electrically neutral (except for ions, when each atom is given an equal charge).

Using this trial density matrix, the one-electron matrix, and the two-electron integrals, a trial fock matrix is constructed.

Diagonalization produces a set of eigen vectors, from which a better density matrix can be made.

This sequence (constructing the density matrix-constructing the Fock matrix diagonalizing the fock to get new eigen vectors) is repeat until the density matrix has became self-consistent to within a pre-set limit.

3.7.4 Calculation of (ΔHf):

The *SCF* calculation produces a density, ***p***; and Fock matrix, ***F***. These together with one- electron matrix, ***H***, allow the total electronic energy to be calculated via:

$$E_{elect}=1/2 \sum_{\sigma}\sum_{\upsilon} P_{\mu\upsilon}(H_{\mu\upsilon}+F_{\sigma\upsilon}) \qquad (3.13)$$

The total core-core repulsion energy is given by

$$E_{nuc}=\sum_{A}\sum_{B<A} E_N(A,B) \qquad (3.14)$$

The additions of these two terms represent the energy released when the ionized atoms and valence electrons combine to form a molecule.

A more useful quantity is the heat of formation of compound from its elements in their standard state. This is obtained when the energy required to ionize the valence electrons of the atoms involved (calculated using semi empirical parameters), E_{isol} (A), and heat of atomization, $E_{atom,}$ are added to the electronic plus nuclear energy this yield:

$$\Delta H_f = E_{elect} + E_{nuc} + \sum E_{isol}(A) + \sum_{A} E_{atom}(A) \qquad (3.15)$$

This is the quantity which Mopac calls ”heat of formation” an alternative but equivalent definition of $\Delta \boldsymbol{H_f}$, more suited for comparison with experimental ΔH_f’s is:

“$\Delta \boldsymbol{H_f}$ is the calculated gas-phase heat of formation at 298K of one mole of a compound from its elements in their standard state”

Chapter Four
Material and Method

4.1 dependence of open circuit voltage on the energy levels of the donor and acceptor material:

Recently the necessity of optimizing the V_{oc} has attracted much attention [16]. There is a need for optimizing the electronic match between the donor and acceptor component, in order to minimize unnecessary internal loss of open circuit voltage.

It has been shown that, within certain limits with respect to the electrodes work function as long as ohmic contacts at both electrodes, the V_{oc} of bulk hetero junction PV cell scales linearly with the decrease of the first reduction of potential of the acceptor [17]. Hence, there is within certain limits [18], a linear relationship between the donor HOMO and acceptor LUMO energy difference and the V_{oc} of the (BHJ) device (see Fig.4.1). Consequently the upper limit for the open circit voltage of bulk heterojunction solar cell is determined by the energy difference of the HOMO of the electron donor and the LUMO of the electron acceptor. It should be noted at this point that for any given donor-acceptor couple as active layer material, minimizing the difference in work function of the two metal electrodes leads to a lowering of V_{oc}, [16].The relation between the V_{oc} and HOMO and LUMO levels is in the form:

$$q(V_{oc} + \Delta V_b) = HOMO_{donor} - LUMO_{acceptor} \qquad (4.1)$$

Where

ΔVb is the sum of the voltage losses at each contact, q is the electronic charge.

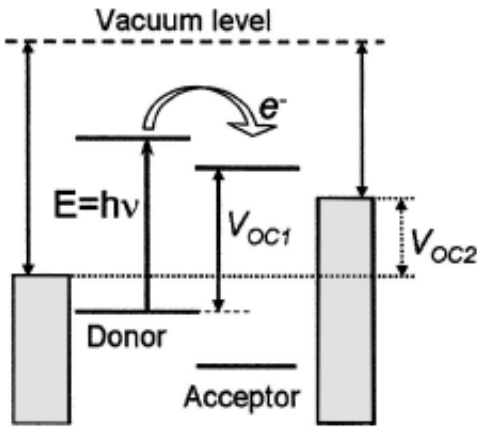

Fig. 4.1 Schematic variation of V_{oc} with acceptor strength ~solid double headed arrow, V_{oc1}) or/and electrode work function ~dotted arrow, V_{oc2}), in a donor/acceptor BHJ solar cell. The electron transfer, occurring at the donor/acceptor interface after light excitation, is indicated by the bent arrow.

Due to the high exciton binding energy in conjugated polymers, light absorption does not lead directly to free charge carriers, but an exciton is created. By mixing in an electron acceptor, it becomes energetically favorable for the electron to jump over to the acceptor, thus breaking up the exciton. This process yields a Coulombically bound electron-hole pair which may dissociate thermally; possibly aided by an electric field, [19]. Fig 4.2 shows the lowest unoccupied molecular orbital LUMO and highest occupied molecular orbital HOMO of P3HT and PCBM. Due to the large offset between the LUMO of the donor, and the LUMO of the acceptor, electron transfer from the donor onto the acceptor takes place, thereby breaking up the exciton. However, the excess energy of the electron and the hole is dissipated quickly. This energetic loss is reflected in the open-circuit voltage *V*oc, which is limited by the difference between the HOMO of the donor and the LUMO of the

acceptor, [19]. The difference offset reduces the output power and, hence, efficiency of the solar cell. Experimental and theoretical investigations of polymer/polymer BHJs show that electron transfer occurs, provided that the difference in LUMO levels is larger than the binding energy of the intrachain exciton,[19], which is known to be approximately 0.4 eV, [19].Since the difference in LUMO levels is much larger than the exciton binding energy, it should be possible to decrease the LUMO(A)-LUMO(D)offset without decreasing the electron transfer efficiency and thereby increasing the energy difference between the HOMO of the donor and the LUMO of the acceptor. The performance of the photovoltaic devices is greatly enhanced by lowering the LUMO (*A*)-LUMO (*D*) offset, primarily caused by an increase in open circuit voltage. For the P3HT/PCBM system, the LUMO (*A*)-LUMO (*D*) offset amounts to 1.1 eV, leading to 3.5% efficiency[19]. Ultimately, by lowering this offset to 0.5 eV the device efficiency would increase to more than 8%, showing the great importance of matching the electronic levels of donor and acceptor.

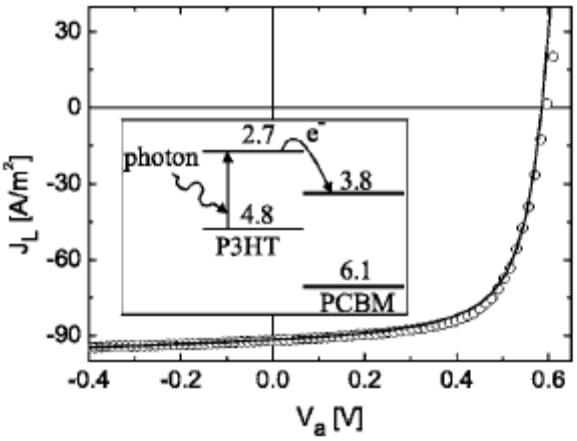

Fig. 4.2 The current-voltage characteristics of a P3HT/PCBM (BHJ) solar cell (symbols) and the fit to the data (line). The inset shows the energy levels, energies given in electron-volts with respect to vacuum, of a P3HT/PCBM BHJ, together with the process of electron transfer from P3HT to PCBM.

In this work we will optimize the V_{oc} by raising the HOMO level and the band gap of the donor in a solar cell consisting of a blend of the (PTs) as a donor material, and the fullerene PCBM as an acceptor one.

4.2 Polythiophene:

Polythiophenes (PTs) result from the polymerization of thiophenes, a sulfur or heterocyclic, which can become conducting when electrons are added or removed from the conjugated π-orbital via doping.

The study of polythiophenes has intensified over the last three decades, [20]. The maturation of field of conducting polymers was confirmed by the a warding of the 2000 Nobel Prize in chemistry to Alan Mac Diarmid and Hideki Shirakawa for the discovery and development of conductive polymers[20]. The most notable property of these materials, electrical conductivity, results from the delocalization of electrons along the polymer backbone. The conductivity is not the only

interesting property resulting from electron delocalizing , the optical properties of the material respond to environmentally stimuli with dramatic color shifts in response to change in solvent, temperature, applied potential, and binding to other molecules. Both color changes and conductivity changes are induced by the same mechanism twisting of the polymer backbone, disrupting conjugation, making conjugated polymers attractive as sensors that can provide a range of optical and electronic responses, [20].

4.3- Mechanism of conductivity and doping:

Electrons are delocalized along the conjugated backbones of conducting polymers, usually through overlap of π-orbital resulting in an extended π-system with a field valance band. By removing electrons from the π-system (p-doping), or adding electrons into the π-system (n-doping), a charge unit called a bipolaron is formed.

Doping is performed at much higher levels (20-40%) in conducting polymers than in semiconductor. The bipolaron moves as a unit up and down the polymer chain, and is responsible for the macroscopically observed conductivity of the polymer, [20].

A variety of reagents have been used to dope PTs. Iodine and bromine produce high conductivities [20], but are unstable and slowly evaporate from the material [20].Organic acid including trifluoroacetic acid, proponic acid, and sulfonic acids produce PTS with lower conductivity than Iodine but with higher stabilities [20].

In this research we use Mopac for semi empirical calculation to optimizing the energy levels of polythiophene by doping it with Iodine and Bromine to replace the hydrogen in the polythiophene backbone. Also we replace the hydrogen with some alkyls, methyl, and hexyl. The

changes in HOMO and LUMO levels and their effect on V_{oc} are discussed in the next chapters.

Chapter Five

Results and calculations

The results of PTs with substitution of an anion material (halogens) and cation material (alkyls), using Mopac and Molda for protein modeling program are shown in Tables 5.1.1, 5.2.1, 5.3.1, 5.4.1, and 5.5.1.

5.1-HOMO and LUMO levels of conducting polythiophene:

Semi empirical calculations were performed on conducting PTs with a 9 unit cells. AM1 Hamiltonian was used and 1SCF was specified. The results are shown in Table 5.1.1.

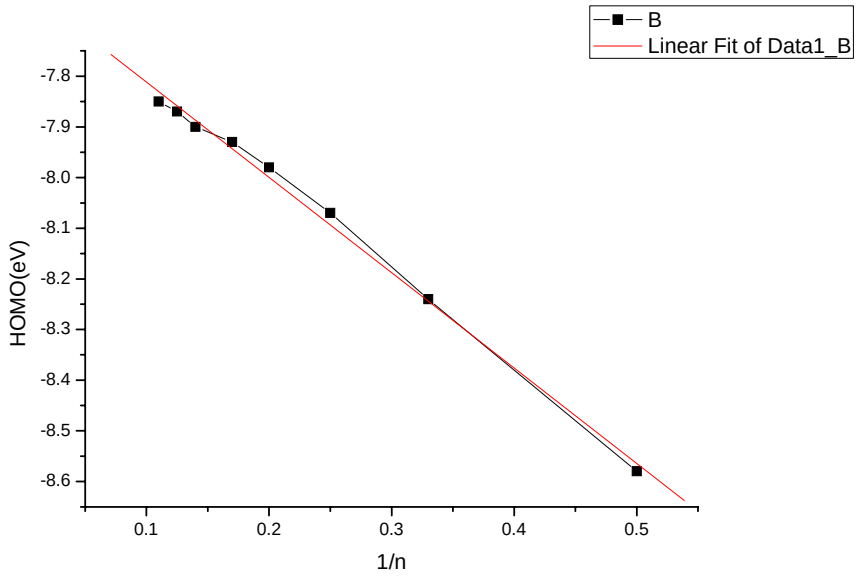

Fig. 5.1.1: The relation between the HOMO level of PTs and 1/n. The straight line is the linear fitting of the data.

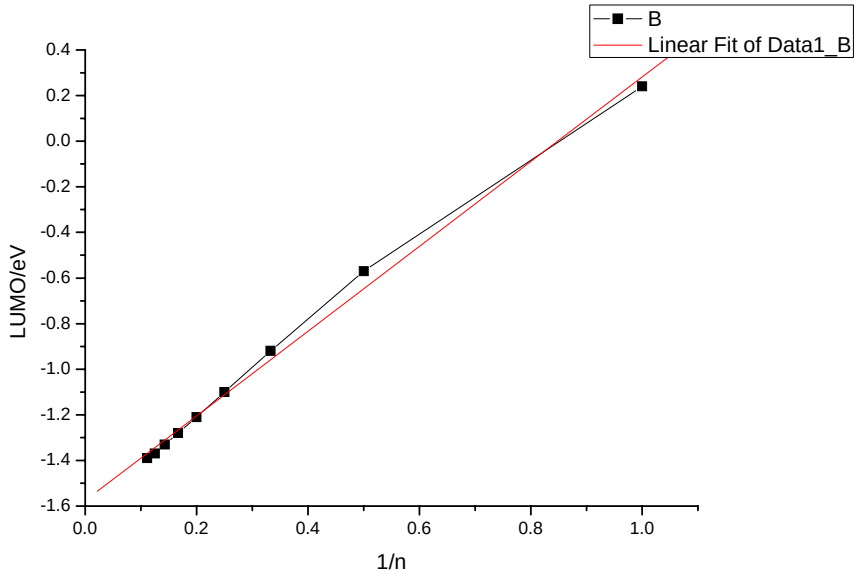

Fig.5.1.2: The relation between the LUMO level of PT and 1/n. The straight line is the linear fitting of the data.

Figs. 5.1.1 and 5.1.2 show the relation between HOMO and LUMO levels and 1/n, where n is the number of repeat unit cell. The linear fitting of the data is a straight line which has the form:

$$Y = A + B * X \qquad (5.1)$$

where A is the intersection from Y axis (HOMO/LUMO) and B is the slop of the line.

Table 5.1.2 the parameters A and B value of conducting PT

Parameter	Value	Error
A	7.62325	0.01389
B	1.88164	0.05357

A gives the value of the HOMO when n approaches ∞.Thus, the semi empirical result of the HOMO level of PTs is:

$$HOMO_{PT} = (7.62325 \pm 0.01389)eV \quad \textbf{(5.1.1)}$$

Table 5.1.3 the parameters A and B of LUMO level of PT

Parameter	Value	Error
A	1.57661	0.02028
B	1.85907	0.04903

$$LUMO_{PT} = (1.57661 \pm 0.02028)eV \quad \textbf{(5.1.2)}$$

Table 5.1.1 conducting polythiophene semi empirical results

No. repeat unit cell (n)	Final heat of formation (Kcal)	Total energy (eV)	Electronic energy (eV)	Core-core repulsion (eV)	Ionization potentials (eV)	No of filled levels	Molecular weight	LUMO (eV)	HOMO (eV)
1	27.44	-760.95	-2548.18	1787.2	9.22	13	84.14	0.24	-9.22
2	56.62	-1494.51	-6935.71	5441.2	8.58	25	166.26	-0.57	-8.58
3	85.77	-2228.07	-12356.7	10128.6	8.23	37	248.38	-0.92	-8.24
4	114.94	-2961.64	-18475.5	15513.9	8.07	49	330.5	-1.10	-8.07
5	144.10	-3695.20	-25122.1	21426.9	7.98	61	412.6	-1.21	-7.98
6	173.27	-4428.76	-32193.4	27764.6	7.92	73	494.74	-1.28	-7.93
7	202.44	-5162.33	-39619.5	34497.2	7.90	85	576.85	-1.33	-7.90
8	231.61	-5895.89	-47353.3	41454.4	7.87	97	658.97	-1.37	-7.87
9	260.78	-6629.45	-55348.2	48718.7	7.86	109	641.09	-1.39	-7.85

5.2 HOMO and LUMO levels of poly3hexylethiophene (P3HT):

Semi empirical calculations were performed on a conducting PT with a 9 unit cells. AM1 Hamiltonian was used and 1SCF was specified.

The HOMO and LUMO levels of PT with a hexyl group substituted for a hydrogen atom in the polymer chain are given in Table 5.2.1.

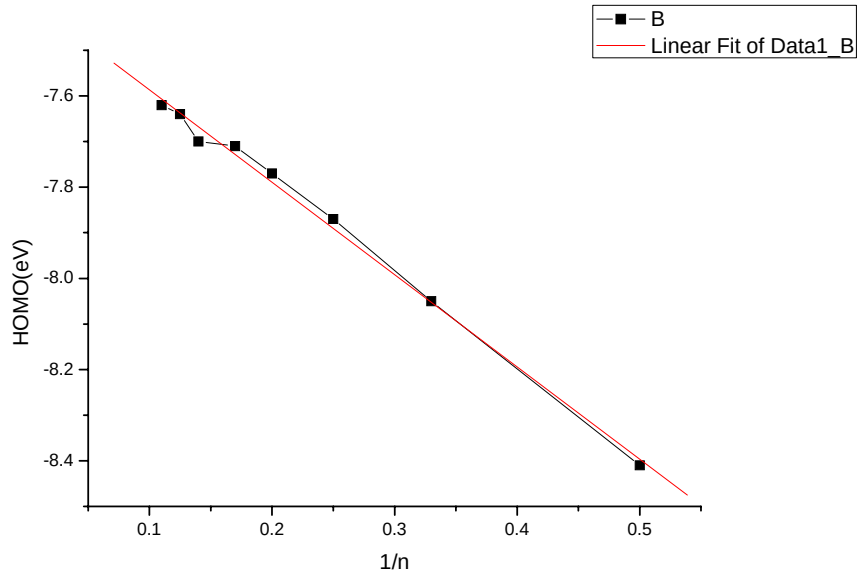

Fig. 5.2.1: The relation between the HOMO level of P3HT and 1/n. The straight line is the linear fitting of the data.

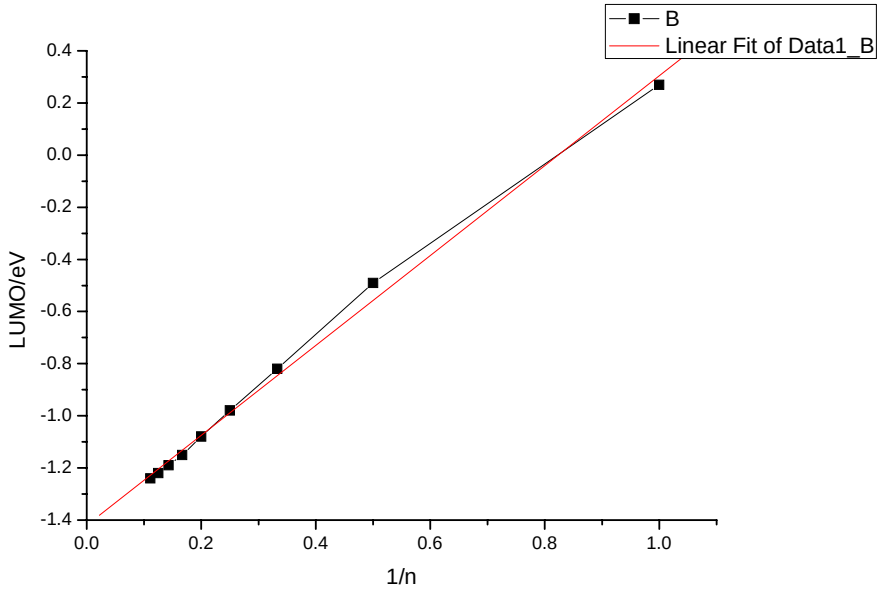

Fig.5.2.2: The relation between the LUMO level of P3HT and 1/n. The straight line is the linear fitting of the data

Table 5.2.2 the parameter A and B value of HOMO level of P3HT

Parameter	Value	Error
A	7.38455	0.01529
B	2.02391	0.05897

The semi empirical value of the HOMO level of P3HT is:

$$HOMO_{P3HT} = (7.38455 \pm 0.01529)eV \qquad \textbf{(5.2.1)}$$

Table 5.2.3 the parameter A and B value of LUMO level of P3HT

Parameter	Value	Error
A	1.41996	0.01681
B	1.72479	0.04065

$$LUMO_{P3HT} = (1.41996 \pm 0.01681)eV \qquad \textbf{(5.2.2)}$$

Table 5.2.1 poly3hexylethiophene (P3HT) semi empirical results:

No repeat unit cell	Final heat of formation (Kcal)	Total energy (eV)	Electronic energy (eV)	Core-core repulsion (eV)	Ionization potentials (eV)	No of filled levels	Molecular weight	LUMO (eV)	HOMO (eV)
1	-13.48	-1695.9	-9152.4	7456.5	8.95	31	168.30	0.27	-8.95
2	-24.78	-3364.5	-25045.5	21681.0	8.41	61	334.58	-0.49	-8.41
3	-36.19	-5033.0	-46847.4	41814.4	8.05	91	500.86	-0.82	-8.05
4	-47.60	-6701.6	-72349.2	65647.6	7.87	121	667.14	-0.98	-7.87
5	-59.01	-8370.1	-101078.6	92708.5	7.77	151	833.42	-1.08	-7.77
6	-70.43	-10038.7	-132272.8	12234.1	7.71	181	999.70	-1.15	-7.71
7	-81.84	-11707.2	-165666.7	153959.5	7.70	211	1165.98	-1.19	-7.70
8	-93.26	-13375.8	-200891.8	187516.0	7.64	241	1332.36	-1.22	-7.64
9	-104.7	-15044.3	-237779.9	222735.6	7.62	271	1498.54	-1.24	-7.62

5.3 HOMO and LUMO levels of poly3methylthiophene (P3MT):

Semi empirical calculations were performed on a conducting PT with a 9 unit cells. AM1 Hamiltonian was used and 1SCF was specified.

The HOMO and LUMO levels of PT with a methyl group substituted for a hydrogen atom in the polymer chain are given in Table 5.3.1.

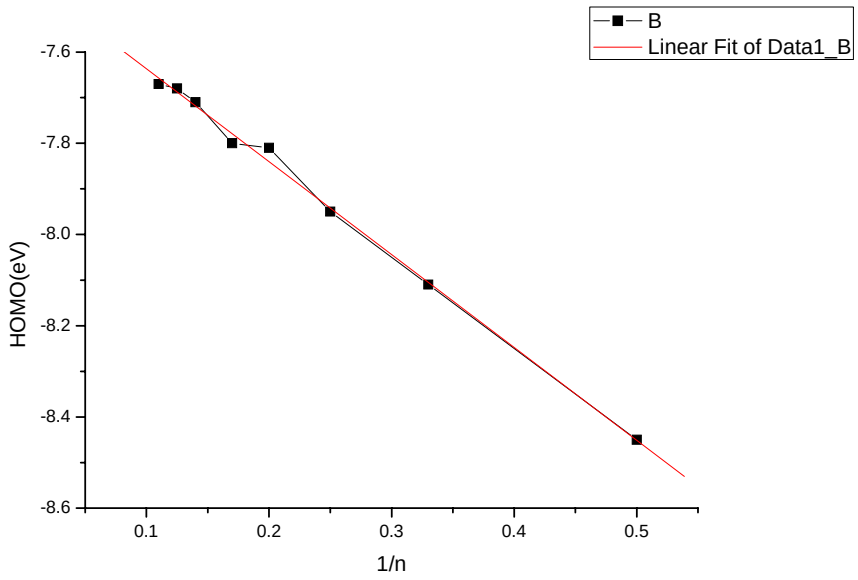

Fig. 5.3.1: The relation between the HOMO level of P3MT and 1/n, the straight line is the linear fitting of the data.

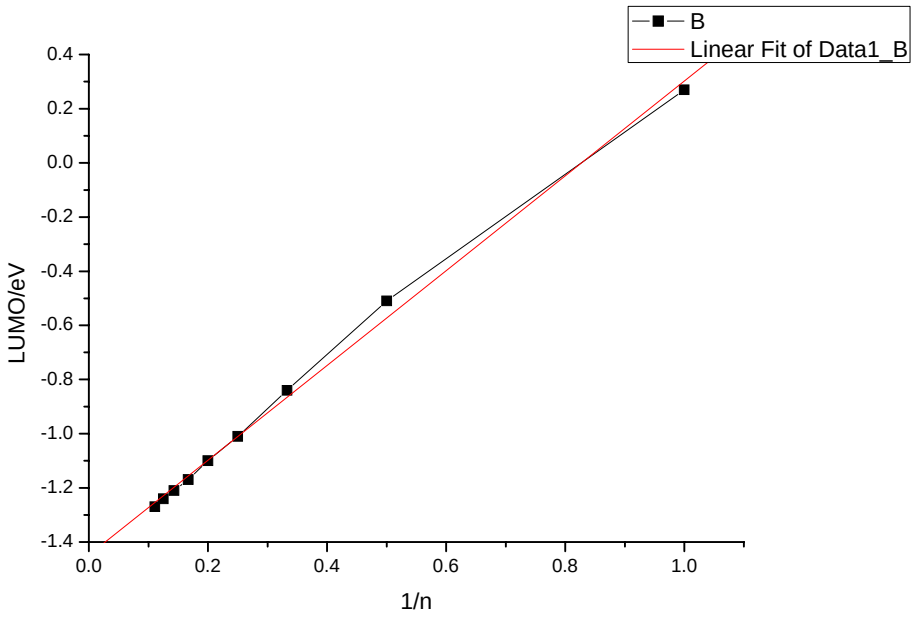

Fig.5.3.2: the relation between the LUMO level of P3MT and 1/n. The straight line is the linear fitting of the data.

Table 5.3.2 the parameter A and B value of HOMO level of P3MT

Parameter	Value	Error
A	7.43303	0.01264
B	2.03602	0.04876

The semi empirical value of the HOMO level of P3MT is:

$$HOMO_{P3MT} = (7.43303 \pm 0.01264)ev \qquad \textbf{(5.3.1)}$$

Table 5.1.3 the parameters A and B of LUMO level of P3MT

Parameter	Value	Error
A	1.44784	0.01547
B	1.74994	0.0374

$$LUMO_{P3MT} = (1.44784 \pm 0.01547)eV \qquad \textbf{(5.3.2)}$$

Table 5.3.1 poly3methylthiophene (P3MT) semi empirical results:

No repeat unit cell (n)	Final heat of formation (Kcal)	Total energy (eV)	Electronic energy (eV)	Core-core repulsion (eV)	Ionization potentials (eV)	No of filled levels	Molecular weight	LUMO (eV)	HOMO (eV)
1	19.31	-916.84	-3494.8	2577.9	8.96	16	98.2	0.27	-8.96
2	41.59	-1806.2	-9672.3	7866.1	8.45	31	194.3	-0.51	-8.45
3	63,81	-2695.6	-17462.8	14767.1	8.11	46	290.5	-0.84	-8.11
4	68,03	-3585.1	-26332.6	22747.6	7.95	61	386.6	-1.01	-7.95
5	105.2	-4474.6	-36174.8	31700.0	7.81	76	482.7	-1.10	-7.81
6	130.5	-5363.8	-46386.5	41022.6	7,80	91	578.9	-1.17	-7.80
7	148.1	-6253.4	-57532.3	51278.9	7.71	106	675.0	-1.21	-7.71
8	170.3	-7142.8	-68886.7	61743.9	7.68	121	771.2	-1.24	-7.68
9	192.5	-8032.2	-80686.4	72654.1	7.67	136	867.3	-1.27	-7.67

5.4 HOMO and LUMO levels of poly3yodothiophene (P3BrT):

Semi empirical calculations were performed on a conducting PT with a 9 unit cells. AM1 Hamiltonian was used and 1SCF was specified.

The HOMO and LUMO levels of PT with Iodine atom substituted for a hydrogen atom in the polymer chain are given in Table 5.4.1.

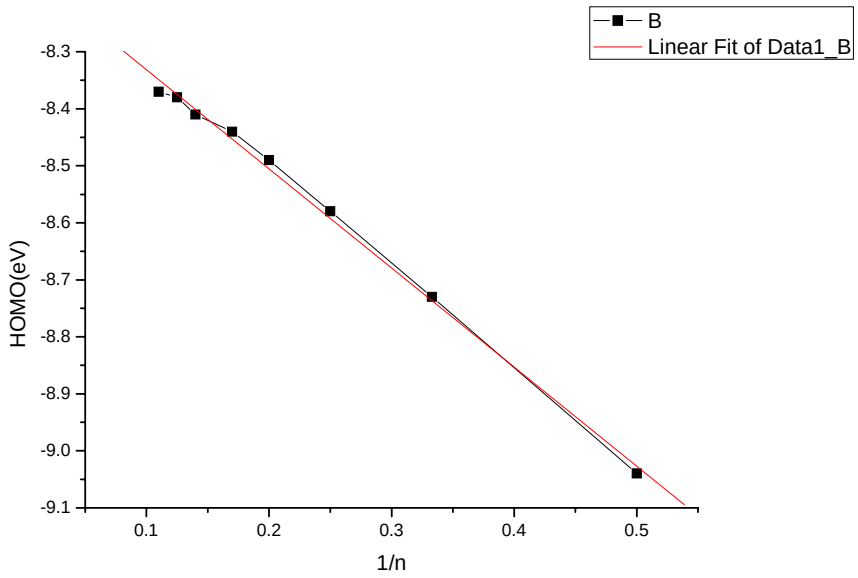

Figure 5.4.1: The relation between the HOMO level of P3IT and 1/n, the straight line is the linear fitting of the data.

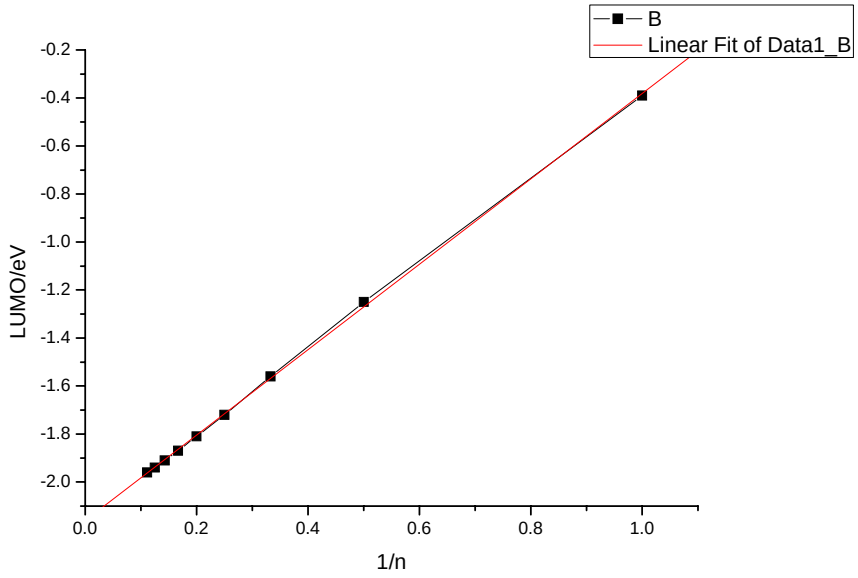

Fig.5.4.2: the relation between the LUMO level of P3IT and 1/n. The straight line is the linear fitting of the data.

Table 5.4.2 the parameter A and B of HOMO level of P3IT

parameter	Value	Error
A	8.15775	0.01106
B	1.73849	0.04259

The semi empirical value of the HOMO level of P3BrT is:

$$HOMO_{P3BrT} = (8.15775 \pm 0.01106)eV \qquad \textbf{(5.4.1)}$$

Table 5.4.3 the parameters A and B of LUMO level of P3IT

parameter	Value	Error
A	2.16058	0.00511
B	1.77979	0.01235

$$LUMO_{P3BrT} = (2.16058 \pm 0.00511)eV \qquad \textbf{(5.4.2)}$$

Table 5.4.1 poly3bromothiophene (P3IT) semi empirical results:

No repeat unit cell (n)	Final heat of formation (Kcal)	Total energy (eV)	Electronic energy (eV)	Core-core repulsion (eV)	Ionization potentials (eV)	No of filled levels	Molecular weight	LUMO (eV)	HOMO (eV)
1	34.91	-1440.26	-4625.8	3185.57	9.34	19	241.9	-0.39	-9.34
2	68.49	-2853.27	-12949.4	10096.2	9.04	37	481.8	-1.25	-9.04
3	101.73	-4266.29	-23664.9	19398.6	8.73	55	721.8	-1.56	-8.73
4	134.98	-5679.31	-35928.4	30249.1	8.58	73	961.7	-1.72	-8.58
5	168.24	-7092.33	-49394.3	42302.0	8.49	91	1201.6	-1.81	-8.49
6	201.49	-8505.36	-63813.2	55307.8	8.44	109	1441.5	-1.87	-8.44
7	234.74	-9916.38	-79036.2	69117.8	8.41	127	1681.4	-1.91	-8.41
8	268.00	-11331.4	-94945.1	83613.7	8.38	145	1921.3	-1.94	-8.38
9	301.26	-12744.4	-111458.	98713.8	8.37	163	2161.2	-1.61	-8.37

5.5 HOMO and LUMO levels of poly3Bromothiophene (P3IT):

Semi empirical calculations were performed on a conducting PT with a 9 unit cells. AM1 Hamiltonian was used and 1SCF was specified.

The HOMO and LUMO level of PT with bromine atom substituted for a hydrogen atom in the polymer chain are given in Table 5.5.1.

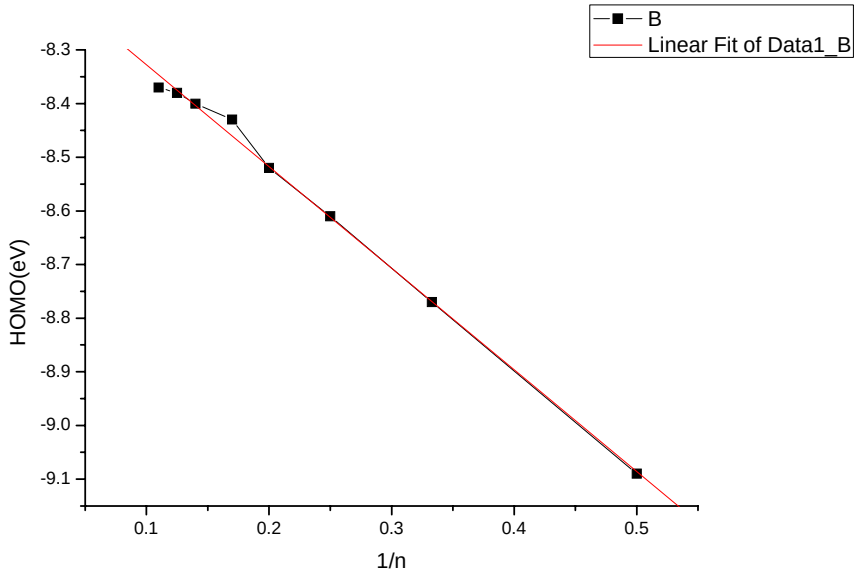

Figure 5.5.1: The relation between the HOMO level of P3BrT and 1/n, the straight line is the linear fitting of the data.

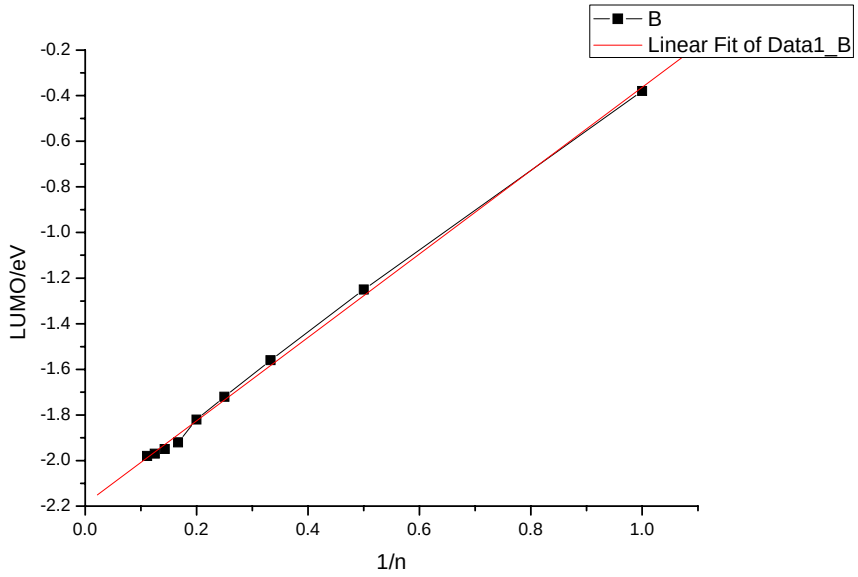

Fig.5.5.2: the relation between the LUMO level of P3BrT and 1/n. The straight line is the linear fitting of the data.

Table 5.5.2 the parameters A and B of the HOMO level of P3BrT

Parameter	Value	Error
A	**8.13837**	**0.01189**
B	**1.89446**	**0.04579**

The semi empirical value of the HOMO level of P3IT is:

$$HOMO_{P3IT} = (8.13837 \pm 0.01189)eV \quad \textbf{(5.5.1)}$$

Table 5.5.3 the parameters A and B of LUMO level of P3BrT

Parameter	Value	Error
A	2.19158	0.01138
B	1.82894	0 02752

$$LUMO_{P3IT} = (2.19158 \pm 0.01138)eV \quad \textbf{(5.5.2)}$$

Table 5.5.1 poly3Yodothiophene (P3BrT) semi empirical results:

No repeat unit cell (n)	Final heat of formation (Kcal)	Total energy (eV)	Electronic energy (eV)	Core-core repulsion (eV)	Ionization potentials (eV)	No of filled levels	Molecular weight	LUMO (eV)	HOMO (eV)
1	56.43	-1428.3	-4544.6	3116.3	9.45	19	335.9	-0.38	-9.45
2	109.39	-2829.5	-12772.3	9942.8	9.09	37	669.8	-1.25	-9.09
3	161.87	-4230.7	-23398.2	19167.6	8.77	55	1003.8	-1.56	-8.77
4	214.38	-5631.9	-35572.3	29940.5	8.61	73	1337.7	-1.72	-8.61
5	266.91	-7033.0	-48950.5	41917.5	8.52	91	1671.6	-1.82	-8.52
6	319.42	-8434.2	-63281.9	54847.8	8.43	127	2005.5	-1.92	-8.43
7	371.94	-9835.4	-78418.0	68582.6	8.40	145	2339.4	-1.95	-8.40
8	424.47	-11236.6	-94240.3	83003.7	8.38	163	2673.3	-1.97	-8.38
9	476.99	-12637.8	110666.9	98029.1	8.37	181	3007.2	-1.98	-8.37

5.6 Approximation used to match the energy levels of the semi empirical results (HOMO-LUMO) with the experimental values:

The theoretical results are matched with the experimental values to obtain a correction relationship. The experimental values of HOMO and LUMO are compared with semi empirical result from Mopac by using Am1 Hamiltonian. The values of the HOMO and LUMO of (P3HT), reported of the literature are 4.8 and 2.7eV, respectively, [46]. The semi empirical results obtained here of the HOMO and LUMO, when n is infinity, are 7.39and 1.42eV.

Assume that the relation between the experimental and computational value is in the form:

$$E_x = AE_c + B \qquad \textbf{(5.6)}$$

where

Ex =experimental value

E_c=computational value

A and B=constant

By substitute the HOMO and LUMO values for P3HT in Eq. (5.6)

$$\begin{aligned} 4.8 &= 7.39A + B \\ 2.7 &= 1.42A + B \end{aligned} \qquad (5.7)$$

$$A = 0.352 \qquad (5.8)$$

$$B = 2.199 \qquad (5.9)$$

Thus from Eq.5.8 and Eq.5.9

$$Ex = 0.352Ec + 2.199 \qquad (5.10)$$

This final equation can be used to correct the semi empirical result of energy level for all polythiophene derivatives. It is valid only when n goes to infinity.

From Eq.5.10 the HOMO and LUMO levels of the PT, P3HT, P3MT, P3BrT, and P3IT are given in Table 5.6:

Table 5.6: the corrected value of the HOMO and LUMO levels of PTs

Name of polymer derivative	PT	P3HT	P3MT	P3BrT	P3IT
HOMO(eV)	4.88	4.80	4.82	5.06	5.07
LUMO(eV)	2.75	2.70	2.71	2.96	2.97
Band gap(eV)	2.13	2.10	2.11	2.10	2.10

From the result above we found that there is no change in band gap for both alkyls and halogens substitution in conducting PT, but the energy levels were shifted down in vacuum with halogens substitution, and shifted up with alkyls substitution, see Fig.5.6

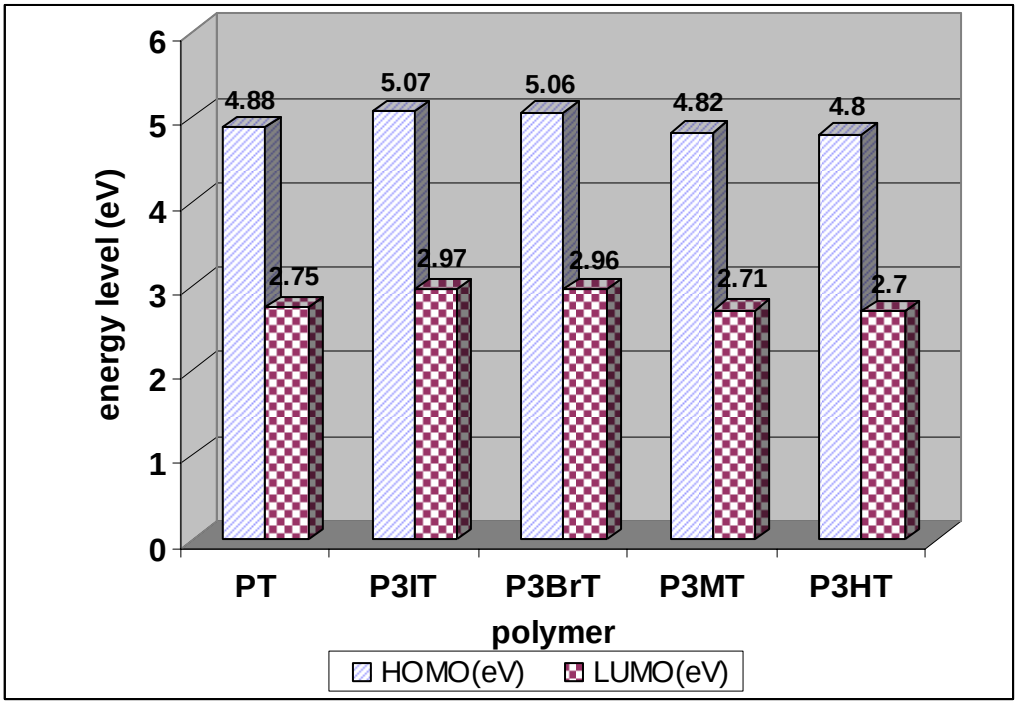

Fig.5.6 schematic diagram of the HOMO and LUMO for the polymers PT, P3HT, P3MT, P3BrT, and P3IT.

5.7 calculation of percentage solar cell efficiency:

To calculate the efficiency of the solar cells, combine Eq.2.37 and Eq.4.1

$$\eta_e = (HOMO_D - LUMO_A - q\Delta V_b)\frac{* I_{sc} * FF}{qP_{in}} \qquad (5.11)$$

From this equation the efficiency is directly proportional to the difference between the HOMO of the donor and the LUMO of the acceptor. The value of $q\Delta V_b = 0.3eV$ is given by, [21]

$$\eta_e \propto V_{oc} \qquad (5.12)$$

Thus the percentage increase in the open circuit voltage led to percentage increase in the efficiency of the solar cell.

The V_{oc} of the solar cell can be calculated from Eq.5.13.

$$Voc = \frac{HOMO_{donor} - LUMO_{acceptor} - 0.3}{q} \qquad (5.13)$$

And the percentage change in the V_{oc} can be calculated from Eq.5.14

$$\Delta V_{oc} = (V_{oc}^{'} - V_{oc}) / V_{oc} \qquad (5.14)$$

where V'_{oc} is the open circuit voltage of the derivatives and Voc is the open circuit voltage of the intrinsic polymer.

The HOMO and LUMO levels of the PCBM are equal to 6.1, and 3.8eV, respectively.

From Eq.5.13, and Eq.5.14, the Voc and the change resulting from doping of the intrinsic PT are given in Table. 5.7:

Table.5.7. The Voc and the percentage change resulting from doping of the intrinsic PT with alkyls (hexyls, and methyl) and halogens (Br, and I):

Polymer	**(PT: PCBM)**	**(P3HT: PCBM**	**(P3MT: PCBM**	**(P3BrT: PCBM**	**P3IT: PCBM**
Voc (V)	0.78	0.70	0.66	o.96	0.97
ΔVoc %	-	-10.3%.	-15.4%	23.1%.	24.4%

Chapter Six

Conclusion and recommendation

6.1 Theoretical modeling of organic solar cell devices:

The devices used in this study consist of a blend of polylthiophene (PTs) as the donor and 6,6-phenyl C61-butyric acid methyl ester (PCBM) as the acceptor, sandwiched between Indium Tin Oxide(ITO), and an evaporated aluminum (Al)top electrode.

The results show that the efficiency of a solar cell of PT with hexyl group substituted for hydrogen atom is decreased by 10.3%. And with methyl group the decrease is about 15.4% from the cell of intrinsic polythiophene.

The efficiency of the solar cell is increased by 23.1% with Bromine substituted for hydrogen atom in PT, and is increased by 24.4% with Iodine substitution.

Thus the polythiophen with Iodine Substituted for hydrogen gave the best efficiency of this solar cell.

6.2 Recommendation:

In future work we recommend using this semi empirical method to study the electronic structure, band structures and doping for different conducting polymers, and we recommend using the derivative P3IT in the solar cell to enhance the efficiency.

References:

[1] Dipl.Ing. Klaus Petritsch, PhD Thesis, Organic Solar Cell Architectures

Technischen Universit¨at Graz (Austria), Cambridge and Graz, July 2000

[2] D. Adam, F. Closs, T. Frey, D. Funhoff, D. Haarer, H. Ringsdorf, P. Schuhmacher and K. Siemensmeyer ”Transient photoconductivity in a discotic liquid crys- tal.” Phys.Rev.Lett. 70, 457-460 (1993

[3] Valentin Dan Mihailet¸chi, Device Physics of Organic Bulk Heterojunction Solar Cells, Rector Magnificus, dr. F. Zwarts, in het openbaar te verdedigen opmaandag 14 november 2005 om 13.15 uur

[4] M. A. Green, K. Emery, D. L. King, S. Igari,W.Warta, Solar cell efficiency tables (version25), Progress in Photovoltaics **13** (2005), 49.

[5] W. Shockley, H. J. Queisser, Detailed balance limit of efficiency of p-n junction solar cells, Journal of Applied Physics **32** (1961), 510

[6] Green, MA photovoltaic, technology, technology overview Energy policy, 2000, 28 (14): P989.

[7] Green, M.A. Silicon Solar cell-Advanced principle and p particle.1ed.centre of photovoltaic Devices and system, university of New South Wales, Sydney (1995).

[8] Roger A. Messenger Jerry Vetre. Photovoltaic systems engineering, Second Edition. Boca Raton, London. New York Washington, D.C.

[9] Sze, S.M.1993. physics of semiconductor devices Wiley Eatern Limited, New Delhi. Third Edition.

[10]W. Shockley, “The Theory of ***p-n*** Junctions in Semiconductors and ***p-n*** Junction Transistors,” Bell Syst. Tech. J., 28,435 (1949);

.[11]C. T. Sah, R. N. Noyce, and W. Shockley, “Carrier Generation and Recombination in ***p-n*** Junction andp-n Junction Characteristics,” Proc. IRE, **45,** 1228 (1957).

[12]1Yildiz Technical University, Faculty of Arts and Science, Department of Physics, Davutpasa-ISTANBUL2Linz Institute for Organic Solar Cells (LIOS), Johannes Kepler University Linz, Physical Chemistry,

Altenberger Strasse, Linz-AUSTRIA, Geliş/Received: 16.04.2007

[13] Rostalski,J., Meissner,D., Solar Energy Mater. Solar Cells, Vol. 61, 87, 2000.

[14] Conducting Polymer Special report Mercourl G.Kanatizidis Michigan state university,2001.

[15]Mopac 2000 Manual,Revision Number 2, by James J.P Stewart

[16] Floris B. Kooistra, Joop Knol, Fredrik Kastenberg, Lacramioara M. Popescu, Wiljan J. H. Verhees, Jan M. Kroon, and Jan C. Hummelen*,Molecular Electronics, Materials Science CentrePlus, UniVersity of Groningen, Nijenborgh 4, 9747 AG Groningen, The Netherlands, and Energy Research Centre of the Netherlands (ECN), Solar Energy, P.O. Box 1, 1755 ZG Petten, 2007.

[17] Brabec, C. J.; Cravino, A.; Meissner, D.; Sariciftci, N. S.;

Fromherz, T.; Rispens, M. T.; Sanchez, L.; Hummelen, J. C. AdV. Funct. Mater. 2001, *11*, 374.

[18] Frohne, H.; Shaheen, S. E.; Brabec, C. J.;

Mu¨ller, D. C.; Sariciftci, N. S.;Meerholz, K. ChemPhysChem 2002, 795.

[19] L. J. A. Koster,a_ V. D. Mihailetchi, and P. W. M. Blom, Materials Science CentrePlus, University of Groningen, Nijenborgh 4,9747 AG Groningen, The Netherlands, Received 24 October 2005; accepted 24 January 2006; published online 2 March 2006

[20] Richard McCullough group, Carnegie Mellon, Tobin Marks group, Northwestern, John Reynolds group, University of Florida. Timothy Swager group, MIT. Ivan Oleynik group, University of South Florida. Dhandapani Venkataraman group, University of Massachusetts, Amherst. Gregory Sotzing's group, University of Connecticut, Storrs. Jean Frechet's group, Jean Frechet, University of California, Berkeley. Michael McGehee group, Stanford University, polythiophene, Wikipedia , 8 February 2007.

[21] Markus C.Scharber, David M, Markus K, Patriec Denk ,Chriestoph W,Alan.J.Heeger, and Christoph.J.Barbec, Desigen Rules For Donors in bulk-heterojunction solar cell,DOI:10.1002/adama200501717,Advanced Materials

[22]. W. Shockley, Electrons and Holes in Semiconductors, D. Van Nostrand, Princeton, New Jersey, 1950